ACS APPLIED MATERIALS & INTERFACES

www.acsami.org

Research Article

Flexible Tri-switchable Wettability Surface for Versatile Droplet Manipulations

Yuegan Song, Yanlei Hu,* Yachao Zhang, Guoqiang Li,* Dawei Wang, Yi Yang, Yafeng Zhang, Yiyuan Zhang, Wulin Zhu, Jiawen Li, Dong Wu,* and Jiaru Chu

Cite This: *ACS Appl. Mater. Interfaces* 2022, 14, 37248−37256

Read Online

ACCESS | Metrics & More | Article Recommendations | Supporting Information

ABSTRACT: Smart surfaces with tunable wettability are promising due to their abilities to create diversified functionalities that the fixed surfaces cannot provide. However, limited by imprecise adjustment of structural geometry and almost conventional switching modes of wettability, it is still challenging to achieve the reversible switching between multiple wetting states. Herein, a novel tri-switchable wettability surface with an in situ switching ability is used for the manipulation of a given droplet, which consists of a stretchable substrate and a micron column array. The femtosecond laser direct writing technique is utilized to generate distinct wettability of the two components. Taking the advantage of good tensile properties, the surface morphology is adjusted in a rapid, reversible way to obtain diverse wetting performances from the lotus-like effect to rice-leaf-like anisotropy and then to the rose-petal-like effect. Based on the triplex wetting transition on the same surface, we further developed a multifunctional device to realize a range of in situ manipulations, including the surface self-cleaning, the directional transport of droplets, and the capture, the vertical transport, and release of droplets. This work paves the way for expanding the field of smart surfaces with tunable wettability beyond conventional dual-property wetting behavior and exhibits versatile manipulations of droplets for microfluidic applications.

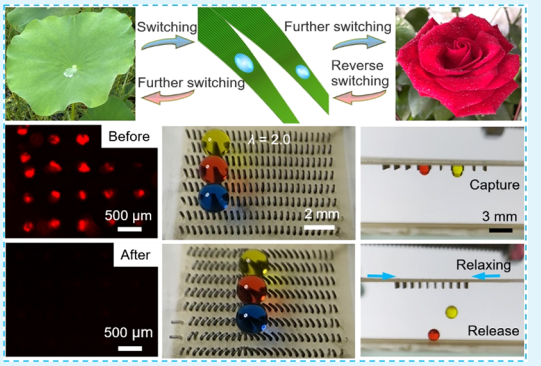

KEYWORDS: *tri-switchable wettability surface, tensile force, femtosecond laser, in situ switching, multifunctional device*

1. INTRODUCTION

Great contributions have been made to human production and life by imitating the surface wettability of specific organisms to realize desirable functions, such as biomimetic lotus leaf surfaces for self-cleaning,[1−6] anisotropic functional surfaces inspired by rice leaves,[7−11] and highly adhesive superhydrophobic surfaces imitating the rose petal pinning effect.[12−14] However, the fixed surface that characterizes specific wetting properties and functions is greatly constrained in some cutting-edge applications. The most representative example is the requirement of intelligent devices, such as microfluidic switches and biomedical transporters. Conversely, smart surfaces that enable dynamical switching among different wetting states are highly desirable.

It is known that the wettability on the surface is a result of the synergy between surface micro-/nanostructures and their chemical compositions.[15,16] Therefore, numerous studies have been devoted to regulating surface chemistry by external stimulation to obtain a functional surface with dynamically switchable wettability.[17−21] However, the adjustment processes often have drawbacks such as time-consuming, high cost, poor biocompatibility, and so forth. On the other hand, researchers adjust surface microgeometry to switch the wettability of the surface to obtain new functions.[22−29] Some efforts have been expended on shape memory polymers by virtue of their good shape memory effect, attempting to realize the goal of dynamic wettability switching. Nevertheless, almost all previous studies are focused on tuning the microstructure induced by the cooperative effect of pressure and thermal stimulation.[30−40] Interestingly, some applications such as no-loss transfer of a given droplet require more sensitive in situ switching of surface wettability. For this reason, elastic substrates are widely applied to adjust the surface microstructure dynamically via mechanical strain.[22,26,41−44] Goel et al. reported an anisotropic buckled surface with dual-scale roughness, on which the droplet rolls more easily in the direction parallel to the wrinkles.[41] Wang et al. fabricated an ethylene-vinyl acetate film surface with tunable adhesion by further stretching and demonstrated the pick and transfer of droplets on this basis.[42] Sun et al. prepared a kind of skin-like wearable surface with tunable wettability, which can

Received: July 19, 2022
Accepted: July 22, 2022
Published: August 8, 2022

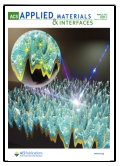

https://doi.org/10.1021/acsami.2c12890
ACS Appl. Mater. Interfaces 2022, 14, 37248−37256

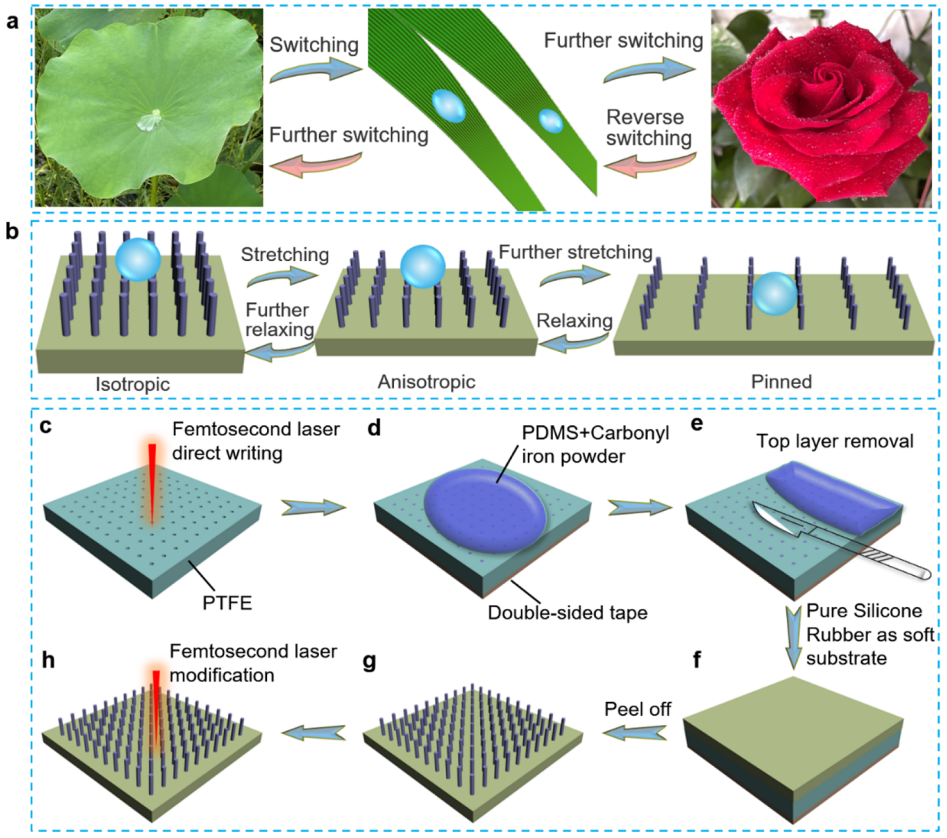

Figure 1. Conceptualization and fabrication of the TSWS. (a,b) Conception and schematic diagram inspired by three typical wetting surface archetypes. (c−h) Schematic illustration of the fabrication procedures of TSWS.

be applied to the joints of the finger to realize controllable capture and release of droplets like tweezers.[26]

Although previous studies have provided successful experiences for switchable wettability surfaces as referred to above, so far, the structures are still confined to dual-property wetting behaviors and switching between them.[17,22−26,37,38,41−44] It is of great significance to widen the switchable multiple wettability on the surface. Also, the surfaces fabricated by the existing preparation methods are either involved in complicated fabrication steps, poor scalability, or limited adjustment capacity. Moreover, it is still challenging for tunable wettability surfaces to realize multidimensional, continuous, and no-loss manipulation of a given droplet in practical applications. Therefore, it is meaningful to develop a surface beyond dual-switchable wetting behavior to realize the refined regulations of micromorphology and wettability, so as to achieve versatile manipulations for the droplet.

In this work, a flexible biomimetic surface that can switch reversibly in situ between triplex wettability states, the lotus-like effect, the rice-leaf-like anisotropy, and the rose-petal-like effect, is explored. The surface consists of a stretchable substrate and a micron column array prepared by the femtosecond laser direct writing and soft transfer technique. By taking advantage of the tensile properties, surface morphology is adjusted rapidly and reversibly to obtain diverse wetting performances. Due to the triplex wetting transition on the same surface, we further developed a functional device to realize a range of in situ manipulations, including the surface self-cleaning, directional transport of droplets, and the capture, vertical transport, and release of droplets. The results reveal great potential in microfluidics, biomedical engineering, and microreactor.

2. RESULTS AND DISCUSSION

2.1. Principle and Preparation of the Smart Surface. Three typical wetting surface archetypes in nature are tactfully integrated to generate a tri-switchable wettability surface (TSWS) with an in situ switching ability (Figure 1a,b). This work consists of six key procedures: first, the femtosecond laser direct writing technique is employed to fabricate a microhole (diameter of 140 μm) array on the polytetrafluoroethylene (PTFE) as a template (Figure 1c). After sticking a double-sided tape tightly to the bottom of PTFE, a mixture of liquid polydimethylsiloxane (PDMS), a hardening agent, and carbonyl iron powder (10:1:4 by weight) is then cast into the template (Figure 1d), which contributes to the transfer of the micron column array. The excess mixture of PDMS and iron powder is removed with a scalpel to facilitate the attachment between the substrate materials and micron column array (Figure 1e). Subsequently, the silicone (A/B = 1:1 by weight) is cast onto the PTFE template to generate an elastic substrate, while the substrate is attached to the micron columns (Figure 1f). After curing in an oven at 130 °C for 30 min, the mold is taken off (Figure 1g). Finally, the expected TSWS is obtained after femtosecond laser modification (Figure 1h).

2.2. Surface Microstructure and Its Wettability. Scanning electron microscopy (SEM) is used to characterize and analyze the change in surface micromorphology to understand surface wettability and its variation. Before laser modification, both the original silicone substrate and the top of the micron columns are relatively smooth (Figure 2a−c). The

https://doi.org/10.1021/acsami.2c12890
ACS Appl. Mater. Interfaces 2022, 14, 37248−37256

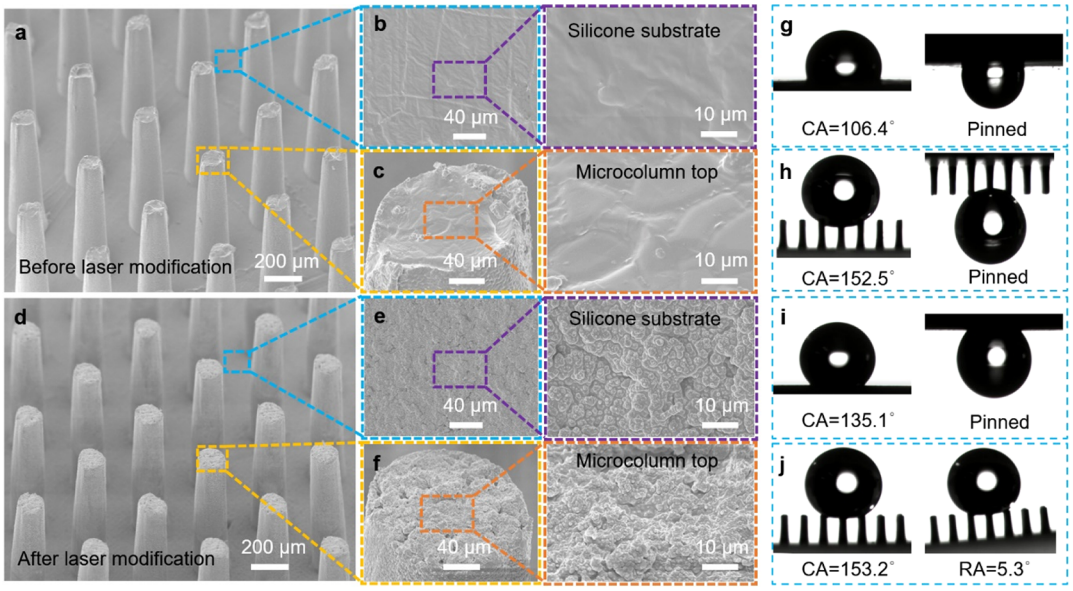

Figure 2. Micromorphology and wettability characterization of TSWS. (a–f) SEM images of the structure before and after laser modification. CA and RA of the silicone substrate (g) before laser modification and (i) after laser modification. CA and RA on the top of the micron column (h) before laser modification and (j) after laser modification. The droplet volume is 4 μL. CA and RA are the average values of the measurements on five samples.

droplet shows hydrophobicity with a contact angle (CA) of ≈106.4° on the flat silicone substrate (Figure 2g), while it exhibits superhydrophobicity (CA ≈ 152.5°) on the top of the micron columns (Figure 2h), ascribing to the Wenzel mode formed at the tip of the micron column array. When the sample is rotated by 180°, the droplet either on the silicone substrate or on the top of the micron column array does not fall off, showing high adhesion (Figure 2g,h).

After laser modification, it is observed that the silicone substrate and the top of the micron columns are uniformly covered by cauliflower-like micro-/nanoparticles (Figure 2d–f), which are produced by laser ablation and the deposition during ablation. Consequently, the hydrophobicity of the silicone substrate is enhanced with a high CA increase of ≈28° (from 106.4 to 135.1°) (Figure 2i). However, the CA (≈153.2°) of the droplet on the top of micron columns hardly changes (Figure 2j), on account of the CA on the micron column surface mainly determined by the micron column array itself instead of the microtopography of its top. Further experiments found that when a 4 μL droplet is enlarged to 12 μL and then shrunk to 6 μL, there is an advancing/a receding CA of 135°/115° on the silicone substrate, while an advancing/a receding CA of 153°/150° on the top of micron columns. From this, the CA hysteresis can be estimated (Figure S1).[45] Meanwhile, as shown in Figure 2i, the droplet remains strongly pinned on the silicone substrate after laser modification not just due to its material properties. According to Wenzel equation, the reason for the phenomena is that the rough surface further increases the actual solid–liquid contact area, which promotes the immersion, resulting in sticky superhydrophobicity. Conversely, the rolling angle (RA) of the droplet on the micron column array is drastically decreased to 5.3° (Figure 2j). Our research shows that after laser modification, there is no variation in both the crystal structure and chemical composition of the PDMS micron columns.[46] It indicates that the decrease in surface adhesion is attributed to the decrease in the contact area of the solid–liquid interface on the top of micron columns arising from the Cassie mode. As a result, the surface of micron columns exhibits superhydrophobicity with low adhesion (Figure S2).

2.3. In Situ Reversible Tri-switching on the Smart Surface. By a simple method of gradually applying or removing the tensile force, the structure can be switched in an in situ reversible manner between the lotus-like effect, the rice-leaf-like anisotropy, and the rose-petal-like effect triplex wettability states (Figures S3–S5). For this reason, first, the tensile properties of the structure are tested. As shown in Figure 3a, upon stretching, the length (L_0) of the structure gradually increases to λL_0, where λ is the stretch ratio. p_x and p_y are the spacing (p) between adjacent micron columns along the x and y axes, respectively. The structure can be stretched to $\lambda = 3$ and recovered its original shape without any breakage or observable deformation after 20 cycles (Figures 3b–d and S6, Video S1), indicating its excellent repeatable tensile properties. Meanwhile, it can be observed that p_x increases with λ, while p_y decreases (Figure 3e). On account of dynamically switchable wettability on the surface, the quantitative relationship between the stretch ratio (λ) and the RAs of droplets along the x-axis (RA_x) and y-axis (RA_y) is shown in Figure 3f,g. Both RA_x and RA_y increase gradually with stretch ratio (λ). What calls for special attention is that the RAs in both directions remain small when p = 400 μm, resulting in the absence of a rose-petal-like effect. When p = 500 μm and $\lambda \geq 2.5$, the droplet can be pinned on the surface. As a comparison, when p = 600 μm and $\lambda = 2$, a rose-petal-like pinned phenomenon appears (Figure S7). The abovementioned analysis results confirm the choice of initial spacing p = 500 μm in the experiment, which contributes to the feasibility of triplex wetting surface design, including the lotus-leaf-like effect with $\lambda = 1$, rice-leaf-like anisotropy with $1 < \lambda < 2.5$, and rose-petal-like effect with $\lambda \geq 2.5$.

In the original state without external force, it can be observed that the silicone substrate is covered by micron

https://doi.org/10.1021/acsami.2c12890
ACS Appl. Mater. Interfaces 2022, 14, 37248–37256

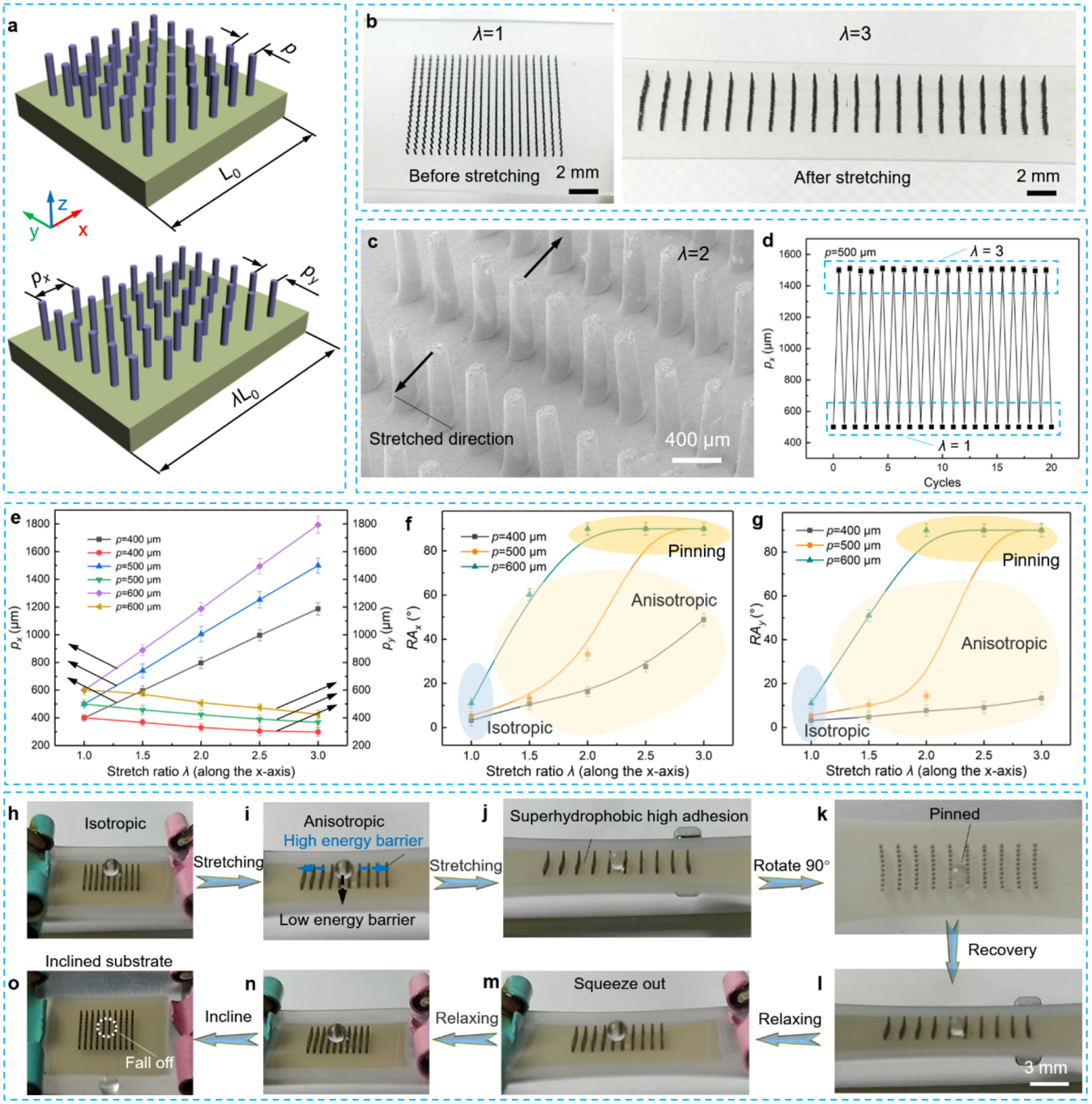

Figure 3. In situ reversible tri-switching on the surface. (a) Three-dimensional (3D) model before and after stretching of the structure. (b) Optical images of the structure before and after stretching. (c) SEM images of the structure after stretching. (d) Stretch and recovery performance tests of the sample with 20 stretch−relax cycles. (e) Quantitative relationship between λ, p_x, and p_y after stretching with different p. The quantitative relationship between (f) λ and RA_x and (g) λ and RA_y. (h−o) Optical images of in situ reversible tri-switching on the surface. Error bars represent standard deviations from five independent sample measurements.

columns with the same spacing along the x and y axes (Figure 3h). The surface of the structure shows a clear lotus-leaf-like surface effect. A droplet (the diameter of droplet d is greater than the spacing of micron columns p) remains spherical on the micron column surface. Meanwhile, there is a similar RA in two directions because of the same energy barrier along the x and y axes (Figures 3h and S3).

After applying the external tensile force, the anisotropy characteristics of the surface tend to be more obvious. The RA of the droplet in the x-axis is always larger than that of the y-axis, resulting in the easier movement of the droplet along the y-axis (Figures 3i and S4). In summary, the adjustment of the microstructure due to the stretching effect endows it a rice-leaf-like anisotropy.

The spacing of micron columns along the x-axis increases with an increasing tensile force. When the diameter of the droplet is smaller than the spacing of the micron columns (p_x) along the x-axis, the droplet comes into full contact with the silicone substrate, where it is strongly pinned due to the high adhesion of the substrate, as shown in Figure 3j. Even if the

https://doi.org/10.1021/acsami.2c12890
ACS Appl. Mater. Interfaces 2022, 14, 37248−37256

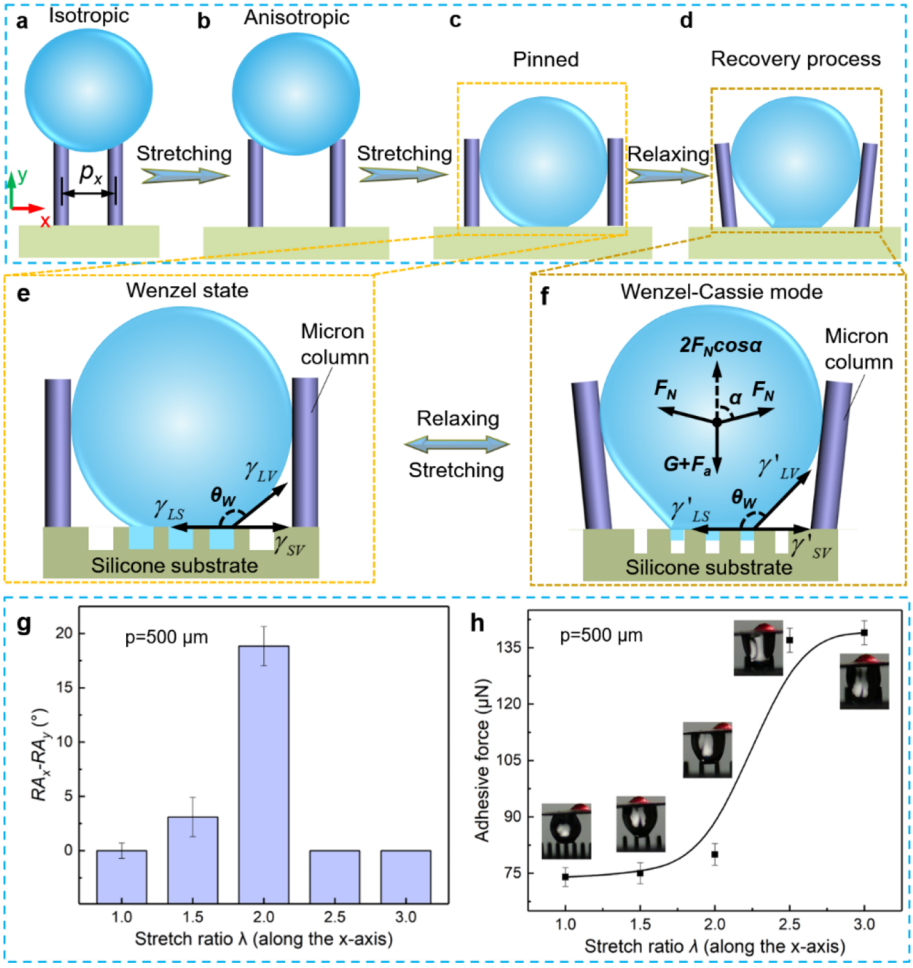

Figure 4. Analysis of the in situ reversible switching mechanism of wetting states on TSWS. (a) Lotus-leaf-like effect. (b) Rice-leaf-like anisotropy. (c) Rose-petal-like effect. (d) Mechanical analysis of the droplet on the surface from a rose-petal-like effect to a rice-leaf-like anisotropy. (e) Droplet exhibits a Wenzel state on the silica substrate. (f) Transition state between Wenzel and Cassie modes as further relaxation. (g) Quantitative relationship between the stretch ratio (λ) and RA difference ($RA_x - RA_y$). (h) Adhesive force to droplets at different stretch ratios (λ). The number (n) of samples used for tests here is $n = 5$, and the average is taken.

sample is rotated by 90°, the droplets do not roll off, indicating that the structure has been successfully switched into a rose-petal-like state (Figures 3k and S5).

As mentioned above, subjected to tensile force, the surface can be switched in situ from the lotus-leaf-like effect to the rice-leaf-like anisotropy and then to the rose-petal-like effect. Subsequently, it is observed that after slowly reducing the tensile force, a reversible switching of wetting states is demonstrated. As shown in Figure 3l, the spacing (p_x) of micron columns along the x-axis decreases with the tensile force. When $p_x < d$, the droplet is squeezed out from the groove back to the top of the micron columns (Figure 3m). The structure is switched back to an anisotropic mode (Figure 3n). Upon further reducing the tension force until it is completely released, it can be observed that the given droplet falls off instantly from the surface affected by the gravitational force when it is tilted, confirming an in situ transition of wetting modes to the lotus-leaf-like surface (Figure 3o and Video S2).

2.4. Mechanism of the Wettability Switching. As described above, it can be observed that by utilizing wettability differences between the two components and the excellent tensile property, the structure is handily endowed with tri-switchable wettability. To obtain a good insight into the transition mechanism, the explanations are as follows:

On the original surface without an external tensile force ($\lambda = 1$), the droplet is situated on the already prepared surface where micron columns are arranged with equal spacing along the x and y axes. It is worth noting that the same intercolumniation contributes to similar energy barriers, prompting the droplet to roll in the direction of the two axes without priority. As a result, the structure represents a lotus-leaf-like state with isotropy and superhydrophobic low adhesion (Figure 4a). After the application of tensile force ($1 < \lambda < 2.5$), the intercolumniation along the x-axis increases gradually, generating the anisotropic micron column array surface (Figure 4b). The measurement of RA also confirms that it is larger in the x-axis direction than the y-axis. The larger intercolumniation corresponds to large energy barriers and vice versa. Therefore, the droplet will roll along the y-axis direction as long as the diameter of the droplet (d) is larger than p_x. By further increasing the tensile force until $d \leq p_x$, the droplet rolls into grooves between the micron columns, creating a pinning state like the rose-petal-like effect, as shown in Figure 4c ($2.5 \leq \lambda \leq 3$). Herein, the support force F from the silicone substrate to the droplet is equal to the gravity (G) of the droplet. In this

https://doi.org/10.1021/acsami.2c12890
ACS Appl. Mater. Interfaces 2022, 14, 37248−37256

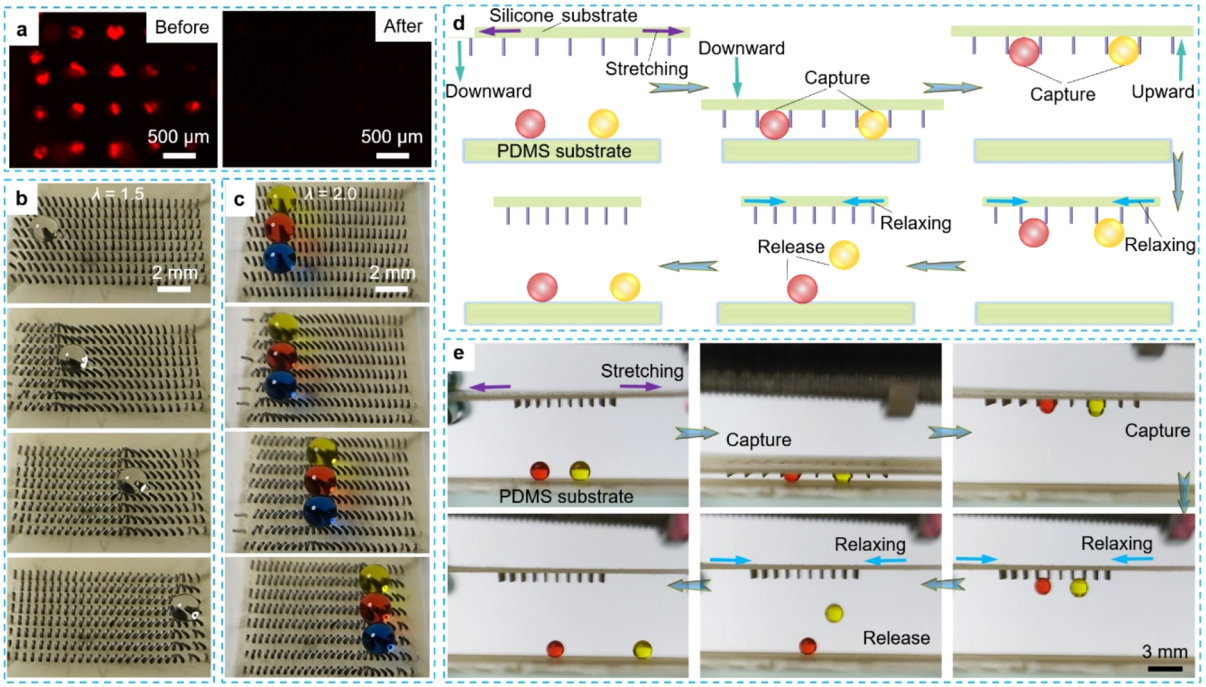

Figure 5. Device for diversified manipulations of droplets is demonstrated. (a) Surface self-cleaning. (b) Directional transport of a 2 μL droplet and (c) parallel transport of multiple 3 μL droplets. (d,e) Schematic diagram and optical images of the capture, vertical transport, and release of a 2 μL droplet.

situation, the droplet partly insets into the silicone substrate with a Wenzel state, as shown in Figure 4e.

Further decreasing the tensile force, when $d > p_x$, and the resultant force (F_0) upon the droplet satisfies eq 1

$$2\gamma'_{LV}\sin\theta_W + 2F_N\cos a > G + F_a \quad (1)$$

where γ'_{LV} is the corrected vapor−liquid interfacial tension, θ_W is the apparent CA of droplet on the silicone substrate, F_N is the extrusion force from micron columns on both sides, F_a is the adhesion between the substrate and the droplet, and $2F_N\cos\theta$ is the upward component of the extrusion force. It is manifested that there is a critical force to promote the switching from the Wenzel mode to a transition state and then to the Cassie mode, when $F_0 > G + F_a$, as shown in Figure 4d,f. Therefore, following the droplet transferred from the silicone substrate to the top of the micron columns, the structure is restored to the rice-leaf-like anisotropic state. Upon relaxation, the surface switches back to the initial lotus-leaf-like effect.

As a validation, we further studied the quantitative relationship between the stretch ratio (λ) and the RA difference ($RA_x - RA_y$), as shown in Figure 4g. The RA difference ($RA_x - RA_y$) is equal to 0° ($\lambda = 1$), showing a lotus-leaf-like isotropy. With the increase in λ ($1 < \lambda < 2.5$), the RA difference ($RA_x - RA_y$) increases first and decreases later, corresponding to the same trend of surface anisotropy. Upon further stretching ($2.5 \leq \lambda \leq 3$), the RA difference ($RA_x - RA_y$) remains at 0°, resulting from high adhesion of the rose-petal-like state.

Also, the adhesive force to the droplet at different stretch ratios (λ) is measured (Figure 4h). The tests find that the adhesive force to the droplet is ~74 μN on the surface of micron columns when $\lambda = 1$. As λ increases ($1 < \lambda < 2.5$), there is little change in the adhesive force to the droplet. However, when $2.5 \leq \lambda \leq 3$, there is a high increase of adhesion to ~140 μN.

2.5. Multifunctional In Situ Manipulation Device of the Droplet. A smart device that possesses abilities for diversified manipulations of droplets and permits reversible switching between them, which is highly desired for microfluidics, is achieved here.

First, to verify the self-cleaning effect of the original structure, a comparative experiment is designed to test the antifouling performance of the micron column surface. The two samples, before and after laser modification, are completely immersed in rhodamine solution for 5 min. As shown in Figure 5a, in contrast to the surface before laser modification, there is no rhodamine residue observed on the modified surface, showing superior antifouling and self-cleaning performances in the original lotus-leaf-effect state.

A droplet is added to further assess the anisotropic wetting effects under tensile control, and the sample is first stretched to $\lambda = 1.5$. Due to the presence of carbonyl iron powder within the micron column, it can be observed that the droplet is transported by directional waves generated by the real-time reconstruction of the micron column array under the magnetic field (Figures 5b and S8 and Video S3). After further stretching to $\lambda = 2.0$, parallel transport of multiple droplets is realized, as shown in Figure 5c (Video S4).

Based on the above-constructed design, the device can be further used as a freely retractable "manipulator" for the capture, vertical transport, and release of the droplets (Figure 5d,e). The device is turned upside-down, and two droplets are placed on the PDMS superhydrophobic film below it as preparation. Upon further stretching to $\lambda = 2.5$ ($d < p_x$), the device is moved down until it reaches the position where the droplets can come into contact with the silicone substrate with high adhesion. Sequentially, the capture of the droplets is realized. Then, the device is moved upward to the target position to complete the vertical transport of the droplets. Finally, as the tensile force decreases, the droplets are squeezed

https://doi.org/10.1021/acsami.2c12890
ACS Appl. Mater. Interfaces 2022, 14, 37248−37256

out to release. From the abovementioned data, it can be inferred that based on the surface, diversified manipulations of droplets are achieved by its triplex wettability switch in an in situ reversible mode, including the surface self-cleaning, droplet directional transport, and the capture, vertical transport, and release of the droplet without limitation (Video S5).

3. CONCLUSIONS

In conclusion, a novel smart surface with the ability to switch between the lotus-like effect, the rice-leaf-like anisotropy, and the rose-petal-like effect in an in situ reversible way is readily prepared and manipulated. The femtosecond laser direct writing and soft transfer techniques are utilized for creating tunable micro-/nanostructures that contribute to distinct wettability with in situ reversible switching capabilities. Based on this, the triplex controllable wettability is tactfully subjected to the variation of the microstructure induced by a simple way to apply or remove the tensile force. Moreover, on account of the splendid multiple wettability, multifunctional droplet manipulations are demonstrated. This work paves the way for expanding the field of smart surfaces with tunable wettability beyond conventional dual-property wetting behavior and exhibits versatile manipulations of droplets for microfluidic applications.

4. EXPERIMENTAL SECTION

4.1. Materials. PTFE is obtained from Dupont China Holding Co., Ltd. Liquid PDMS was provided by Sylgard 184, Dow Corning. Carbonyl iron powder was purchased from Nangong Ruiteng Alloy Material Co., Ltd, with a diameter of 3−5 μm (purity ≥99.9%). Silicone was selected from Beijing Angelcrete Art Landscaping Co., Ltd. The magnets used in this work were purchased from Shanghai Ze He Mechanical & Electrical Co., Ltd.

4.2. Fabrication of the Structure. The microhole (diameter of 140 μm) array on the PTFE (thickness of 800 μm) is fabricated by the femtosecond laser direct writing technique (300 mW, 20 mm/s, 350 times) and used as a template. The double-sided tape is stuck tightly at the bottom of the PTFE template to prevent the leakage of the liquid PDMS during transfer printing. Subsequently, a mixture (10:1:4 by weight) of liquid PDMS, a hardening agent, and carbonyl iron powder (C = 40%) is poured into the PTFE template. After being degassed for 10 min in a vacuum pump, the excess mixture of PDMS and iron powder is removed with a scalpel. After the silicone (A/B = 1:1 by weight, Dragon Skin 10 Slow) is cast onto the PTFE template and degassed in a vacuum pump for 5 min, a homogenizer is used to spin the coating for 60 s at a speed of 500 rpm. After curing in an oven at 130 °C for 30 min, the mold is peeled off carefully. The structure without laser modification is obtained. After femtosecond laser (laser power of 200 mW and scanning speed of 30 mm/s) modification by cross grid lines, the expected in situ tunable wettability surface is fabricated.

4.3. Instrumentation and Characterization. The processing of microholes on the template and modification scanning of the sample are carried out by the femtosecond laser technique. The laser beams are from a regenerative-amplified Ti:sapphire femtosecond laser system (Legend Elite-1K-HE, Coherent) with a repetition rate of 1 kHz, a pulse width of 104 fs, and a center wavelength of 800 nm. The microstructures are characterized by SEM (JSM-6700F SEM, JEOL Ltd., Japan). A CA measurement instrument (CA100C, Shanghai Innuo Precision Instrument Co. Ltd., China) is used to characterize the CAs and RAs of the droplets on the surface. The number (n) of samples used for tests is n = 5, and the average is taken.

ASSOCIATED CONTENT

Supporting Information

The Supporting Information is available free of charge at https://pubs.acs.org/doi/10.1021/acsami.2c12890.

Optical images of characterization of advancing and receding CAs; wettability characteristics on the micron column array surface after laser modification; lotus-like effect on the structure; rice-leaf-like anisotropy on the structure; rose-petal-like effect on the structure; SEM images of the structure after stretching to λ = 1.5; quantitative relationship between RA and p along the x and y axes after stretching; and magnetically responsive bending properties of micron columns on the rice-leaf-like anisotropy surface for droplet transport (PDF)

Cyclic stretching test of TSWS (AVI)

In situ reversible tri-switchable wetting states (AVI)

Droplet transport on the anisotropic surfaces (AVI)

Three droplets moving in parallel (AVI)

Capture, vertical transfer, and release of droplets (AVI)

AUTHOR INFORMATION

Corresponding Authors

Yanlei Hu − *CAS Key Laboratory of Mechanical Behavior and Design of Materials, Key Laboratory of Precision Scientific Instrumentation of Anhui Higher Education Institutes, Department of Precision Machinery and Precision Instrumentation, University of Science and Technology of China, Hefei 230026, P. R. China;* orcid.org/0000-0003-1964-0043; Email: huyl@ustc.edu.cn

Guoqiang Li − *School of Manufacture Science and Engineering, Key Laboratory of Testing Technology for Manufacturing Process, Ministry of Education, Southwest University of Science and Technology, Mianyang 621010, P. R. China;* orcid.org/0000-0001-8161-2065; Email: guoqli@swust.edu.cn

Dong Wu − *CAS Key Laboratory of Mechanical Behavior and Design of Materials, Key Laboratory of Precision Scientific Instrumentation of Anhui Higher Education Institutes, Department of Precision Machinery and Precision Instrumentation, University of Science and Technology of China, Hefei 230026, P. R. China;* orcid.org/0000-0003-0623-1515; Email: dongwu@ustc.edu.cn

Authors

Yuegan Song − *School of Manufacture Science and Engineering, Key Laboratory of Testing Technology for Manufacturing Process, Ministry of Education, Southwest University of Science and Technology, Mianyang 621010, P. R. China; CAS Key Laboratory of Mechanical Behavior and Design of Materials, Key Laboratory of Precision Scientific Instrumentation of Anhui Higher Education Institutes, Department of Precision Machinery and Precision Instrumentation, University of Science and Technology of China, Hefei 230026, P. R. China;* orcid.org/0000-0002-8645-9984

Yachao Zhang − *CAS Key Laboratory of Mechanical Behavior and Design of Materials, Key Laboratory of Precision Scientific Instrumentation of Anhui Higher Education Institutes, Department of Precision Machinery and Precision Instrumentation, University of Science and Technology of China, Hefei 230026, P. R. China*

https://doi.org/10.1021/acsami.2c12890
ACS Appl. Mater. Interfaces 2022, 14, 37248−37256

Dawei Wang − *CAS Key Laboratory of Mechanical Behavior and Design of Materials, Key Laboratory of Precision Scientific Instrumentation of Anhui Higher Education Institutes, Department of Precision Machinery and Precision Instrumentation, University of Science and Technology of China, Hefei 230026, P. R. China*

Yi Yang − *School of Manufacture Science and Engineering, Key Laboratory of Testing Technology for Manufacturing Process, Ministry of Education, Southwest University of Science and Technology, Mianyang 621010, P. R. China*

Yafeng Zhang − *School of Manufacture Science and Engineering, Key Laboratory of Testing Technology for Manufacturing Process, Ministry of Education, Southwest University of Science and Technology, Mianyang 621010, P. R. China*

Yiyuan Zhang − *CAS Key Laboratory of Mechanical Behavior and Design of Materials, Key Laboratory of Precision Scientific Instrumentation of Anhui Higher Education Institutes, Department of Precision Machinery and Precision Instrumentation, University of Science and Technology of China, Hefei 230026, P. R. China;* orcid.org/0000-0002-0393-2597

Wulin Zhu − *CAS Key Laboratory of Mechanical Behavior and Design of Materials, Key Laboratory of Precision Scientific Instrumentation of Anhui Higher Education Institutes, Department of Precision Machinery and Precision Instrumentation, University of Science and Technology of China, Hefei 230026, P. R. China*

Jiawen Li − *CAS Key Laboratory of Mechanical Behavior and Design of Materials, Key Laboratory of Precision Scientific Instrumentation of Anhui Higher Education Institutes, Department of Precision Machinery and Precision Instrumentation, University of Science and Technology of China, Hefei 230026, P. R. China;* orcid.org/0000-0003-3950-6212

Jiaru Chu − *CAS Key Laboratory of Mechanical Behavior and Design of Materials, Key Laboratory of Precision Scientific Instrumentation of Anhui Higher Education Institutes, Department of Precision Machinery and Precision Instrumentation, University of Science and Technology of China, Hefei 230026, P. R. China;* orcid.org/0000-0001-6472-8103

Complete contact information is available at: https://pubs.acs.org/10.1021/acsami.2c12890

Notes

The authors declare no competing financial interest.

■ ACKNOWLEDGMENTS

This work was supported by the National Natural Science Foundation of China (nos. 51875544, 91963127, 52105492, 52122511, and 51605463), the Fundamental Research Funds for the Central Universities (WK2090000024), the Open Fund of the Key Laboratory of Icing and Anti/Deicing (IADL20210408), the Sichuan Science and Technology Program (22cxrc0069), and the Natural Science Foundation of Southwest University of Science and Technology (21zx7136). We acknowledge the Experimental Center of Engineering and Material Sciences at USTC for the fabrication and measurement of samples. This work was partly carried out at the USTC Center for Micro and Nanoscale Research and Fabrication.

■ REFERENCES

(1) Lu, Y.; Sathasivam, S.; Song, J.; Crick, C. R.; Carmalt, C. J.; Parkin, I. P. Robust Self-Cleaning Surfaces that Function When Exposed to Either Air or Oil. *Science* **2015**, *347*, 1132−1135.

(2) Li, X.; Jiang, C.; Zhao, F.; Shao, Y.; Ying, Y.; Ping, J. A Self-Charging Device with Bionic Self-Cleaning Interface for Energy Harvesting. *Nano Energy* **2020**, *73*, 104738.

(3) Cheng, Q.; Li, M.; Zheng, Y.; Su, B.; Wang, S.; Jiang, L. Janus Interface Materials: Superhydrophobic Air/Solid Interface and Superoleophobic Water/Solid Interface Inspired by a Lotus Leaf. *Soft Matter* **2011**, *7*, 5948−5951.

(4) Samaha, M. A.; Tafreshi, H. V.; Gad-el-Hak, M. Superhydrophobic Surfaces: From the Lotus Leaf to the Submarine. *C. R. Mec.* **2012**, *340*, 18−34.

(5) Li, S.; Huang, J.; Chen, Z.; Chen, G.; Lai, Y. A Review on Special Wettability Textiles: Theoretical Models, Fabrication Technologies and Multifunctional Applications. *J. Mater. Chem. A* **2017**, *5*, 31−55.

(6) Tang, M.; Shim, V.; Pan, Z.; Choo, Y.; Hong, M. Laser Ablation of Metal Substrates for Super-Hydrophobic Effect. *J. Laser Micro/Nanoeng.* **2011**, *6*, 6.

(7) Dai, X.; Sun, N.; Nielsen, S. O.; Stogin, B. B.; Wang, J.; Yang, S.; Wong, T.-S. Hydrophilic Directional Slippery Rough Surfaces for Water Harvesting. *Sci. Adv.* **2018**, *4*, No. eaaq0919.

(8) Kang, S. M.; Lee, C.; Kim, H. N.; Lee, B. J.; Lee, J. E.; Kwak, M. K.; Suh, K.-Y. Directional Oil Sliding Surfaces with Hierarchical Anisotropic Groove Microstructures. *Adv. Mater.* **2013**, *25*, 5756−5761.

(9) Long, J.; Fan, P.; Jiang, D.; Han, J.; Lin, Y.; Cai, M.; Zhang, H.; Zhong, M. Anisotropic Sliding of Water Droplets on the Superhydrophobic Surfaces with Anisotropic Groove-Like Micro/Nano Structures. *Adv. Mater. Interfaces* **2016**, *3*, 1600641.

(10) Jang, M. Y.; Park, J. W.; Baek, S. Y.; Kim, T. W. Anisotropic Wetting Characteristics of Biomimetic Rice Leaf Surface with Asymmetric Asperities. *J. Nanosci. Nanotechnol.* **2020**, *20*, 4331−4335.

(11) Yang, X.; Zhuang, K.; Lu, Y.; Wang, X. Creation of Topological Ultraslippery Surfaces for Droplet Motion Control. *ACS Nano* **2021**, *15*, 2589−2599.

(12) Choo, S.; Choi, H.-J.; Lee, H. Replication of Rose-Petal Surface Structure Using UV-Nanoimprint Lithography. *Mater. Lett.* **2014**, *121*, 170−173.

(13) Zhang, X.; Yang, G.; Zong, L.; Jiang, M.; Song, Z.; Ma, C.; Zhang, T.; Duan, Y.; Zhang, J. Tough, Ultralight, and Water-Adhesive Graphene/Natural Rubber Latex Hybrid Aerogel with Sandwichlike Cell Wall and Biomimetic Rose-Petal-Like Surface. *ACS Appl. Mater. Interfaces* **2020**, *12*, 1378−1386.

(14) Zong, C.; Hu, M.; Azhar, U.; Chen, X.; Zhang, Y.; Zhang, S.; Lu, C. Smart Copolymer-Functionalized Flexible Surfaces with Photoswitchable Wettability: From Superhydrophobicity with "Rose Petal" Effect to Superhydrophilicity. *ACS Appl. Mater. Interfaces* **2019**, *11*, 25436−25444.

(15) Chen, C.; Liu, M.; Zhang, L.; Hou, Y.; Yu, M.; Fu, S. Mimicking from Rose Petal to Lotus Leaf: Biomimetic Multiscale Hierarchical Particles with Tunable Water Adhesion. *ACS Appl. Mater. Interfaces* **2019**, *11*, 7431−7440.

(16) Xu, P.; Coyle, T. W.; Pershin, L.; Mostaghimi, J. From Lotus Effect to Petal Effect: Tuning the Water Adhesion of Non-Wetting Rare Earth Oxide Coatings. *J. Eur. Ceram. Soc.* **2020**, *40*, 1692−1702.

(17) Laird, E. D.; Bose, R. K.; Qi, H.; Lau, K. K.; Li, C. Y. Electric Field-Induced, Reversible Lotus-to-Rose Transition in Nanohybrid Shish Kebab Paper with Hierarchical Roughness. *ACS Appl. Mater. Interfaces* **2013**, *5*, 12089−12098.

(18) Liu, M.; Jiang, L. Switchable Adhesion on Liquid/Solid Interfaces. *Adv. Funct. Mater.* **2010**, *20*, 3753−3764.

(19) Liu, Y.; Wang, X.; Fei, B.; Hu, H.; Lai, C.; Xin, J. H. Bioinspired, Stimuli-Responsive, Multifunctional Superhydrophobic Surface with Directional Wetting, Adhesion, and Transport of Water. *Adv. Funct. Mater.* **2015**, *25*, 5047−5056.

(20) Xu, Z.; Zhao, Y.; Wang, H.; Zhou, H.; Qin, C.; Wang, X.; Lin, T. Fluorine-Free Superhydrophobic Coatings with pH-induced

Wettability Transition for Controllable Oil-Water Separation. *ACS Appl. Mater. Interfaces* **2016**, *8*, 5661−5667.
(21) Wu, Z. L.; Buguin, A.; Yang, H.; Taulemesse, J.-M.; Le Moigne, N.; Bergeret, A.; Wang, X.; Keller, P. Microstructured Nematic Liquid Crystalline Elastomer Surfaces with Switchable Wetting Properties. *Adv. Funct. Mater.* **2013**, *23*, 3070−3076.
(22) Park, J. K.; Yang, Z.; Kim, S. Black Silicon/Elastomer Composite Surface with Switchable Wettability and Adhesion between Lotus and Rose Petal Effects by Mechanical Strain. *ACS Appl. Mater. Interfaces* **2017**, *9*, 33333−33340.
(23) Lv, T.; Cheng, Z.; Zhang, D.; Zhang, E.; Zhao, Q.; Liu, Y.; Jiang, L. Superhydrophobic Surface With Shape Memory Micro/Nanostructure and Its Application in Rewritable Chip for Droplet Storage. *ACS Nano* **2016**, *10*, 9379−9386.
(24) Wang, J.-N.; Liu, Y.-Q.; Zhang, Y.-L.; Feng, J.; Sun, H.-B. Pneumatic Smart Surfaces with Rapidly Switchable Dominant and Latent Superhydrophobicity. *NPG Asia Mater.* **2018**, *10*, No. e470.
(25) Cheng, Z.; Zhang, D.; Lv, T.; Lai, H.; Zhang, E.; Kang, H.; Wang, Y.; Liu, P.; Liu, Y.; Du, Y.; Dou, S.; Jiang, L. Superhydrophobic Shape Memory Polymer Arrays with Switchable Isotropic/Anisotropic Wetting. *Adv. Funct. Mater.* **2018**, *28*, 1705002.
(26) Wang, J.-N.; Liu, Y.-Q.; Zhang, Y.-L.; Feng, J.; Wang, H.; Yu, Y.-H.; Sun, H.-B. Wearable Superhydrophobic Elastomer Skin with Switchable Wettability. *Adv. Funct. Mater.* **2018**, *28*, 1800625.
(27) Weng, W.; Tenjimbayashi, M.; Hu, W. H.; Naito, M. Evolution of and Disparity among Biomimetic Superhydrophobic Surfaces with Gecko, Petal, and Lotus Effect. *Small* **2022**, *18*, No. e2200349.
(28) Zhao, Y.; Su, Y.; Su, X.; Hou, M.; Hong, M. Directional Sliding of Water: Biomimetic Snake Scale Surfaces. *Opto-Electron. Adv.* **2021**, *4*, 210008.
(29) Yang, Y.; Zhang, Y.; Hu, Y.; Li, G.; Zhang, C.; Song, Y.; Li, L.; Ni, C.; Dai, N.; Cai, Y.; Li, J.; Wu, D.; Chu, J. Femtosecond Laser Regulated Ultrafast Growth of Mushroom-Like Architecture for Oil Repellency and Manipulation. *Nano Lett.* **2021**, *21*, 9301−9309.
(30) Chen, C. M.; Yang, S. Directed Water Shedding on High-Aspect-Ratio Shape Memory Polymer Micropillar Arrays. *Adv. Mater.* **2014**, *26*, 1283−1288.
(31) Cheng, Z.; Zhang, D.; Luo, X.; Lai, H.; Liu, Y.; Jiang, L. Superwetting Shape Memory Microstructure: Smart Wetting Control and Practical Application. *Adv. Mater.* **2021**, *33*, No. e2001718.
(32) Park, J. K.; Kim, S. Droplet Manipulation on a Structured Shape Memory Polymer Surface. *Lab Chip* **2017**, *17*, 1793−1801.
(33) Wang, W.; Salazar, J.; Vahabi, H.; Joshi-Imre, A.; Voit, W. E.; Kota, A. K. Metamorphic Superomniphobic Surfaces. *Adv. Mater.* **2017**, *29*, 1700295.
(34) Wang, Y.; Lai, H.; Cheng, Z.; Zhang, H.; Liu, Y.; Jiang, L. Smart Superhydrophobic Shape Memory Adhesive Surface toward Selective Capture/Release of Microdroplets. *ACS Appl. Mater. Interfaces* **2019**, *11*, 10988−10997.
(35) Lv, T.; Cheng, Z.; Zhang, E.; Kang, H.; Liu, Y.; Jiang, L. Self-Restoration of Superhydrophobicity on Shape Memory Polymer Arrays with Both Crushed Microstructure and Damaged Surface Chemistry. *Small* **2017**, *13*, No. e1503402.
(36) Zhang, D.; Cheng, Z.; Kang, H.; Yu, J.; Liu, Y.; Jiang, L. A Smart Superwetting Surface with Responsivity in Both Surface Chemistry and Microstructure. *Angew. Chem., Int. Ed. Engl.* **2018**, *57*, 3701−3705.
(37) Shao, Y.; Zhao, J.; Fan, Y.; Wan, Z.; Lu, L.; Zhang, Z.; Ming, W.; Ren, L. Shape Memory Superhydrophobic Surface with Switchable Transition between "Lotus Effect" to "Rose Petal Effect". *Chem. Eng. J.* **2020**, *382*, 122989.
(38) Lai, H.; Shang, Y.; Cheng, Z.; Lv, T.; Zhang, E.; Zhang, D.; Wang, J.; Liu, Y. Control of Tip Nanostructure on Superhydrophobic Shape Memory Arrays toward Reversibly Adjusting Water Adhesion. *Adv. Compos. Hybrid Mater.* **2019**, *2*, 753−762.
(39) Li, W.; Liu, J.; Chen, L.; Wei, W.; Qian, K.; Liu, Y.; Leng, J. Application and Development of Shape Memory Micro/Nano Patterns. *Small* **2022**, *18*, No. e2105958.
(40) Zhang, H.; Lai, H.; Cheng, Z.; Zhang, D.; Liu, P.; Li, Y.; Liu, Y. In-Situ Switchable Superhydrophobic Shape Memory Microstructure Patterns with Reversible Wettability and Adhesion. *Appl. Surf. Sci.* **2020**, *525*, 146525.
(41) Goel, P.; Kumar, S.; Sarkar, J.; Singh, J. P. Mechanical Strain Induced Tunable Anisotropic Wetting on Buckled PDMS Silver Nanorods Arrays. *ACS Appl. Mater. Interfaces* **2015**, *7*, 8419−8426.
(42) Wang, Z.; Yuan, L.; Wang, L.; Wu, T. Stretchable Superlyophobic Surfaces for Nearly- Lossless Droplet Transfer. *Sens. Actuators, B* **2017**, *244*, 649−654.
(43) Wong, W. S. Y.; Gutruf, P.; Sriram, S.; Bhaskaran, M.; Wang, Z.; Tricoli, A. Strain Engineering of Wave-like Nanofibers for Dynamically Switchable Adhesive/Repulsive Surfaces. *Adv. Funct. Mater.* **2016**, *26*, 399−407.
(44) Cao, C.; Feng, Y.; Zang, J.; López, G. P.; Zhao, X. Tunable Lotus-Leaf and Rose-Petal Effects via Graphene Paper Origami. *Extreme Mech. Lett.* **2015**, *4*, 18−25.
(45) Lin, Y.; Hu, Z.; Zhang, M.; Xu, T.; Feng, S.; Jiang, L.; Zheng, Y. Magnetically Induced Low Adhesive Direction of Nano/Micropillar Arrays for Microdroplet Transport. *Adv. Funct. Mater.* **2018**, *28*, 1800163.
(46) Song, Y.; Jiang, S.; Li, G.; Zhang, Y.; Wu, H.; Xue, C.; You, H.; Zhang, D.; Cai, Y.; Zhu, J.; Zhu, W.; Li, J.; Hu, Y.; Wu, D.; Chu, J. Cross-Species Bioinspired Anisotropic Surfaces for Active Droplet Transportation Driven by Unidirectional Microcolumn Waves. *ACS Appl. Mater. Interfaces* **2020**, *12*, 42264−42273.

https://doi.org/10.1021/acsami.2c12890
ACS Appl. Mater. Interfaces 2022, 14, 37248−37256